EARTHQUAKE ENGINEERING AND STRUCTURAL DYNAMICS, VOL. 23, 389–411 (1994)

FOURIER AMPLITUDE SPECTRA OF STRONG MOTION ACCELERATION: EXTENSION TO HIGH AND LOW FREQUENCIES

M. D. TRIFUNAC

Department of Civil Engineering, Kaprielian Hall 210, University of Southern California, Los Angeles, CA 90089-2531, U.S.A.

SUMMARY

It is shown how the empirical equations for scaling the Fourier amplitude spectra in the frequency band from ~ 0.1 to 25 Hz can be extended to describe the strong motion amplitudes in a much broader frequency range. At long periods, the proposed equations are in excellent agreement with (1) the seismological and field estimates of permanent ground displacement (near field) and (2) the independent estimates of seismic moment (far field). At high frequencies, $f \geqslant 25$ Hz, the spectral amplitudes can be described by $\exp(-\pi kf)$, where k ranges from 0·02 (near source) to about 0·06 at an epicentral distance of about 200 km. It is also shown how amplification by local soil and geological site conditions can be defined to apply in the same broad frequency range.

INTRODUCTION

The Fourier amplitude spectrum of strong earthquake acceleration is one of the most direct and common functions used to describe the frequency content of strong earthquake shaking.[1] It is used in source mechanism studies, where its amplitudes and the parameters describing its shape can be related to the slip on the fault, the size of the fault and the stress drop on the fault surface.[2–4] In engineering studies, the Fourier spectrum represents the basic input for (1) analyses of local amplification of incident waves by sedimentary[5–8] and soil deposits,[9,10] (2) analyses of the effects of topographic irregularities on surface ground motion amplitudes[11–13] and (3) studies of the soil–structure interaction.[14–16] In direct linear and probabilistic estimates of structural response, the Fourier amplitude spectrum also represents the basic and most direct representation of the driving forces.[17–26] Finally, in seismic risk studies, using the concept of the uniform risk spectrum,[27,28] when the synthetic ground motion is required for non-linear response calculations, the uniform risk Fourier amplitude spectrum, modified for site-specific effects, is the most direct and convenient starting point for construction of synthetic accelerograms.[29]

Since the late 1960s and early 1970s, with the introduction of advanced signal processing methods, which became possible following the availability of digital computers, and with the rapid growth in the number of recorded strong motion accelerograms,[30–34] it became possible to study empirically the dependence of the Fourier spectrum amplitudes in terms of various scaling parameters describing the earthquake source, the transmission path and the recording site conditions. These studies have now reached the level where it will be difficult to make significant future improvements without a major increase in the quality and the quantity of the available strong motion data.[35–38] The main limitations in the current strong motion data base are: (1) limited frequency range (~ 10 Hz to ~ 1 Hz for events with magnitudes near 3·5–4·0; up to ~ 25–0·07 Hz for events of magnitude seven $\geqslant 7$; (2) lack of strong motion recordings for distances greater than about 100 km;[39] (3) lack of an adequate number of sites with detailed known characteristics of the local soil and geological conditions.

There are several main reasons for writing this paper. The first one is to show how it is possible to extrapolate the Fourier spectral amplitudes to the high (towards 100 Hz) and low (towards 0·01 Hz) frequencies, using our current understanding of how spectral amplitudes should behave there. We will also

CCC 0098–8847/94/040389–23

Received 16 October 1992
Revised 20 May 1993

attempt to extrapolate the spectral amplitudes back to the source region, to see whether the results can be reconciled with the overall data on earthquake source mechanisms. In recent years, there has been some interest in trying to describe the 'long-period' ground motions to allow analyses and design of long bridges and tall structures (for periods longer than about 5 sec). The second aim of this work is to use the presently available information, via a preliminary synthesis of all current data, to develop a basis to guide future priorities in the design of strong motion accelerographs,[40] to define the needs for the number and the places of their deployment, and to define the criteria for strong motion data processing[41] and dissemination.[32] Broad band empirical characterization of strong motion amplitudes near earthquake sources (for distances less than, say 100 km) is also essential for many other related and supporting studies which deal with inelastic wave attenuation and improvements in the local and teleseismic magnitude scales and their relative calibration.[42,43]

Seismological studies of spectral amplitudes usually focus on the spectra of shear waves or of surface waves. In earthquake engineering, the spectral amplitudes of the complete signal are required because it is necessary to estimate the extrema and the number of cycles in the structural response.[18–26] Thus, to the extent that the basic waves contribute to or dominate the overall strong ground motion, there will exist similarities and direct relationships between the 'seismological' and 'engineering' analyses of strong ground motion, but in the end only the complete representation, including contributions from all waves, can be used in the design. This work was guided and influenced by the papers on empirical[2] and theoretical[44] descriptions of the functional forms of spectral amplitudes of S-waves, but the scaling parameters and the final equations describing the Fourier spectra given here aim to represent the total strong ground motion.

This study also differs from many seismological analyses in that it uses regression equations in the frequency band from $\sim 0{\cdot}1$ to 25 Hz, and is based on actually recorded strong motion data. Our equations have terms which could be attributed to known trends and properties of the earthquake source, attenuation along the wave path, and the observed ground motion in general, but they actually represent only carefully chosen empirical regression models which all have coefficients and coefficient functions which are significantly different from zero in much of the frequency band being considered. In this paper, these equations are not modified, but we explore how they could be extrapolated to higher ($f > 25$ Hz) and lower ($f \leqslant 0{\cdot}1$ Hz) frequencies.

In contrast, many seismological studies begin with an analysis of far-field body waves, and then assume functional forms for the spectral amplitudes, for example following Brune's[2] shear wave spectra,[45,46] or assume a physical model of the source which then results in the spectral estimates.[47–51] The typical scaling parameters are the seismic moment, M_0, one or two long-period corner frequencies (inversely proportional to the overall source dimensions and to the assumed dimensions of the asperities and barriers), some form of stress drop on the fault plane, and the low-pass filtering characteristics of the surrounding medium[52] or the non-linear phenomena at the tip of the propagating dislocation.[53] Since M_0 determines the long-period spectral amplitudes, while the stress drop characterizes the high frequencies, such models aim to provide the means to interpolate spectral behaviour for the intermediate frequency band. Eventually, these results can be calibrated using the recorded strong motion data[49,51] and their quality finally depends on one's ability to predict M_0 and the stress drop.

STRONG MOTION DATA

The strong motion acceleration data base grew slowly from March 10, 1933, when the first strong motion accelerograms were recorded during the Long Beach ($M = 6{\cdot}3$) earthquake in California. The San Fernando, California, earthquake of February 9, 1971 contributed the first and essential major increment to the strong motion data base. After all accelerograms were digitized, together with selected older recordings between 1933 and 1971, we had 186 uniformly processed free-field strong motion records.[35,36] Following the Imperial Valley (1979), Coalinga (1983) and Morgan Hill (1984) earthquakes in California, the uniformly processed strong motion data base more than doubled, to 493 uniformly processed records. With recent recordings by the Los Angeles strong motion array (1987–1992) and following the Loma Prieta earthquake, when all data are uniformly processed there will be well over 1000 excellent records in the strong motion data base. The

documentation and the exploratory work to determine the local site conditions at all recording stations are progressing very slowly. The local soil and geological site parameters have been collected since 1975, but these data are difficult and expensive to obtain on a routine basis. The most recent studies[10,54,55] could use only 135 sites for which both the local soil and local geological data were available (Table I). The number of recorded accelerograms with complete site characterization is considerably larger, because of many multiple recordings at the same stations.

Table I illustrates the distribution of the recording sites for which the local geological classification s ($s = 0$ for sediments, $s = 1$ for intermediate sites and $s = 2$ for sites on basement rock[56]) and the local soil classification s_L ($s_L = 0$ for 'rock', $s_L = 1$ for stiff soil sites and $s_L = 2$ for deep soil sites[9]) are available. Sites designated by $s = 0$ have been further described by the thickness of sedimentary deposits, h (km). The soil classification is determined as follows. Rock sites ($s_L = 0$) are where the soil thickness is less than 30 ft (10 m). Stiff soil sites have a soil layer of 50–200 ft (15–70 m) deep. Deep soil sites have a soil layer deeper than 300 ft (100 m), but both have a shear wave velocity less than 2500 ft/sec (800 m/sec). For soil site classification, all materials with shear wave velocity in excess of 2500 ft/sec (800 m/sec) are described as rock.

EMPIRICAL SCALING EQUATIONS

Our most detailed and recent equation for scaling the Fourier amplitude spectra, $FS(T)$ is of the form

$$\log_{10} FS(T) = M + \mathrm{Att}(\Delta, M, T) + b_1(T)M + b_2(T)h + b_3(T)v + b_4(T)hv + b_5(T) + b_6(T)M^2 + b_7^{(1)}(T)S_L^{(1)} + b_7^{(2)}(T)S_L^{(2)} \quad (1)$$

where M is earthquake magnitude,[42,57] $b_1(T)$–$b_7^{(2)}(T)$ are scaling coefficient functions of the period T, and $\mathrm{Att}(\Delta, M, T)$ is the frequency-dependent attenuation function,[39]

$$\mathrm{Att}(\Delta, M, T) = \begin{cases} \mathscr{A}_0(T)\log_{10}\Delta, & R \leqslant R_0 \\ \mathscr{A}_0(T)\log_{10}\Delta_0 - (R - R_0)/200, & R > R_0 \end{cases} \quad (2)$$

with Δ, the 'representative' source to station distance,[49]

$$\Delta = S \ln\left[\frac{R^2 + H^2 + S^2}{R^2 + H^2 + S_0^2}\right]^{-1/2} \quad (3)$$

and Δ_0 equal to Δ when $R = R_0$. When S/R and S_0/R becomes small $\Delta \to (H^2 + R^2)^{1/2}$, which is the hypocentral distance. $\mathrm{Att}(\Delta, M, T)$ depends on M implicitly through S, which is the linearized estimate of the 'source dimension'

$$S = 0{\cdot}2 + 8{\cdot}51(M - 3) \quad \text{for } M > 3 \quad (4)$$

S_0 is the coherence radius of the source and is approximated by $S_0 \sim \beta T/2$, where β is the shear wave velocity in the source region, and T is the period of motion. $\mathscr{A}_0(T)$ is represented by a parabola versus $\log_{10} T$, between $T = 0{\cdot}04$ and $1{\cdot}8$ sec. It is near -2 for $T = 0{\cdot}04$ and it increases to $\sim -0{\cdot}7$ and remains constant for $T \geqslant 1{\cdot}8$ sec.[58] R_0 is the 'transition' epicentral distance[39] (about 150 km for $T < 0{\cdot}05$, and ~ 50 km for $T > 1$ sec) beyond which the attenuation equation has a slope equal to $-1/200$. R is the epicentral distance and H is the focal depth (both are in units of km).

In equation (1), h represents the thickness of the sedimentary layers, from the ground surface to the basement rock (km). The parameter v can have values of 0 or 1. ($v = 0$ for horizontal motion and $v = 1$ for vertical motion). The term $b_4(T)hv$ has been introduced to model the progressively steeper incidence of body waves for soft and deeper sedimentary sites. $b_1(T)M$ and $b_6(T)M^2$ model the saturation of strong motion amplitudes versus M, for $-b_1(T)/[2b_6(T)] \equiv M_{\min} < M < M_{\max} = -[1 + b_1(T)]/[2b_6(T)]$. $S_L^{(1)}$ and $S_L^{(2)}$ are two indicator variables defined by

$$S_L^{(1)} = \begin{cases} 1 & \text{if } s_L = 1 \text{ (stiff soil)} \\ 0 & \text{otherwise} \end{cases} \quad \text{and} \quad S_L^{(2)} = \begin{cases} 1 & \text{if } s_L = 2 \text{ (deep soil)} \\ 0 & \text{otherwise} \end{cases} \quad (5)$$

Table I. Distribution of s and s_L parameters describing local geological and soil conditions for the present data base

	Geological site conditions		
Soil site conditions	Sediments ($s = 0$)	Intermediate sites ($s = 1$)	Basement rock ($s = 2$)
Deep soil, $s_L = 2$	44	2	0
Stiff soil, $s_L = 1$	37	24	3
Rocks, $s_L = 0$	1	11	13

where $s_L = 0, 1$ and 2 represent 'rock', stiff soil and deep soil sites. The sites with soft to medium clays with strata of sands and gravels[9] are not common in the Western United States and are therefore not considered in this analysis.

With $\widehat{FS}(T)$ representing the Fourier amplitude spectra estimated from equation (1) and $FS(T)$ indicating the spectra computed from recorded accelerograms, the residues can be calculated from

$$\varepsilon(T) = \log_{10} FS(T) - \log_{10} \widehat{FS}(T) \tag{6}$$

where $\varepsilon(T)$ can be described by a normal distribution function with mean $\mu(T)$ and standard deviation $\sigma(T)$ as follows:

$$p(\varepsilon, T) = \frac{1}{\sigma(T)\sqrt{2\pi}} \int_{-\infty}^{\varepsilon(T)} \exp\left\{ -\frac{1}{2}\left[\frac{x - \mu(T)}{\sigma(T)}\right]^2 \right\} dx \tag{7}$$

where $p(\varepsilon, T)$ represents the probability that $\log_{10} FS(T) - \log_{10}\widehat{FS}(T) \leqslant \varepsilon(T)$. Table II gives $b_1(T)$–$b_7^{(2)}(T)$, M_{min}, M_{max}, $\mu(T)$ and $\sigma(T)$ at 12 periods $T(1) = 0{\cdot}04$–$T(12) = 14{\cdot}0$ s (for $N = 1, 2, \ldots, 12$).

The first empirical model for scaling $\log_{10} FS(T)$ that involves the frequency dependent attenuation $\mathrm{Att}(\Delta, M, T)$ was developed in 1985, but without explicit consideration of the soil site parameter s_L.[37,58] Simultaneously with that analysis, and with the model described above by equation (1), we also studied the geological site conditions using $s = 0, 1$ and 2 (in place of h). The reader may wish to peruse the details on how these models have evolved, starting with our analysis in 1976 (Reference 35), but for the purposes of this paper it will suffice to recognize only the four most recent models:

1. MAG-SITE,[58]
2. MAG-DEPTH,[58]
3. MAG-SITE-SOIL,[55]
4. MAG-DEPTH-SOIL[54] [equation (1)].

In what follows, we consider these four models simultaneously and refer to them as the 'group of four' most recent scaling models (G4RM). In the above models, MAG implies scaling in terms of earthquake magnitude,[42] SITE indicates the use of the geological site parameters $s = 0, 1$ or 2, and DEPTH implies the use of h as in equation (1) above. SOIL shows that the soil site parameters $s_L = 0, 1$ and 2 are used in the scaling equation. In models 1 and 2, such dependence is omitted.

Figure 1 illustrates $\log_{10} FS(T)$ plotted versus frequency, $f = 1/T$. It shows Fourier amplitude spectra (broken lines) for a probability of exceedance equal to 50 per cent [$p(\varepsilon, T) = 0{\cdot}5$ in equation (7)] and for $M = 4, 5, 6, 7$ and 8. The top shaded area shows the region where the empirical equation (1) is valid [$1/T(N_c) < f < 25$ Hz]. Table III shows the cut-off periods, $T(N_c)$, versus magnitude. For uniformity, all G4RM empirical equations are defined for 12 periods $T(N)$, $N = 1, \ldots, 12$, but can be used only for $N \leqslant N_c$ (see Tables II and III). For long periods, the spectral amplitudes computed from equation (1) are valid up to

Table II. $\log_{10} FS(T) = M_< + \mathrm{Att}(\Delta,M,T) + b_1(T)M_{<>} + b_2(T)h + b_3(T)v + b_4(T)hv + b_5(T) + b_6(T)M^2_{<>} + b_7^{(1)}(T)S_L^{(1)} + b_7^{(2)}(T)S_L^{(2)}$

N	1	2	3	4	5	6	7	8	9	10	11	12
Period, T(sec)	0·040	0·065	0·11	0·19	0·34	0·50	0·90	1·60	2·80	4·40	7·50	14·0
Coefficients												
$b_1(T)$	0·652	0·667	0·819	0·962	0·977	0·927	0·854	0·876	0·940	0·856	0·382	− 0·707
$b_2(T)$	0·067	0·063	0·056	0·047	0·040	0·039	0·049	0·067	0·084	0·087	0·069	0·020
$b_3(T)$	0·127	0·091	− 0·012	− 0·155	− 0·272	− 0·292	− 0·233	− 0·152	− 0·122	− 0·126	− 0·132	− 0·131
$b_4(T)$	0·006	− 0·002	− 0·015	− 0·030	− 0·041	− 0·047	− 0·051	− 0·048	− 0·040	− 0·033	− 0·030	− 0·034
$b_5(T)$	− 3·921	− 3·876	− 4.151	− 4·532	− 4·809	− 4·924	− 5·151	− 5·568	− 5·881	− 5·529	− 3·791	− 0·019
$b_6(T)$	− 0·095	− 0·098	− 0·114	− 0·127	− 0·128	− 0·123	− 0·112	− 0·110	− 0·113	− 0·010	− 0·080	− 0·006
$b_7^{(1)}(T)$	− 0·314	− 0·282	− 0·219	0·120	− 0·008	0·052	0·120	0·161	0·161	0·127	0·065	− 0·002
$b_7^{(2)}(T)$	− 0·264	− 0·260	− 0·238	− 0·151	− 0·012	0·069	0·144	0·169	0·152	0·103	0·004	− 0·144
$M_{\min}$	3·429	3·389	3·604	3·780	3·810	3·773	3·814	3·991	4·155	3·897	2·376	0·000
$M_{\max}$	8·691	8·472	8·006	7·711	7.711	7·845	8·282	8·549	8·576	8·450	8·600	14·500
$\mu(T)$	− 0·002	− 0·002	− 0·002	− 0·001	− 0·001	− 0·001	− 0·002	− 0·001	0·002	0·003	0·001	− 0·001
$\sigma(T)$	0·445	0·462	0·388	0·343	0·316	0·317	0·338	0·352	0·343	0·328	0·315	0·305

Note: $M_< = \min(M, M_{\max}), M_{<>} = \max(M_{\min}, M_<)$.

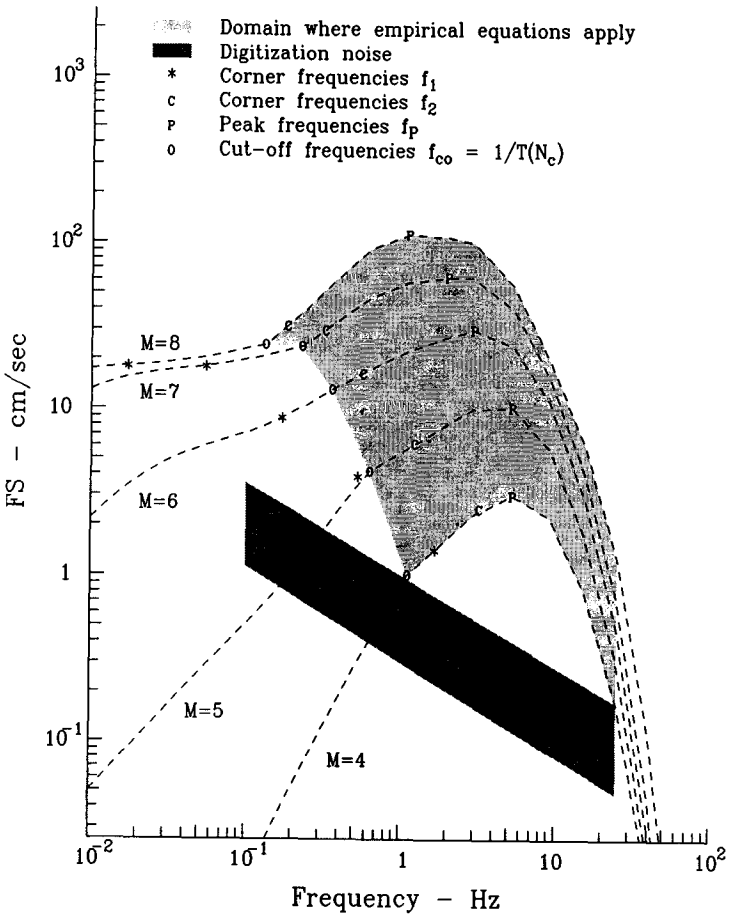

Figure 1. Fourier amplitude spectra (cm/sec) versus frequency (Hz) for probability of exceedance equal to 0·5, for $M = 4, 5, 6, 7$ and 8 (bottom to top), at epicentral distance $R = 10$ km and for source at $H = 0$ depth. Outside the top shaded region, between $f_{co} = 1/T(N_c)$ and $f = 25$ Hz, where equation (1) is valid, the spectral amplitudes (broken lines) can be extrapolated as proposed in this paper. The corner frequencies, f_1 and f_2, and the frequency f_{co} are defined in the text. The processing and digitization noise amplitudes are shown by the (bottom) shaded zone increasing from $FS \sim 10^{-1}$ to $FS \sim 1$ in./sec ($2{\cdot}5 \times 10^{-1}$ to 2·5 cm/sec) for frequencies decreasing from 10 to 0·1 Hz

Table III. Cut-off periods $T(N_c)$ versus magnitude

M	$T(N_c)$	N_c
3	0·90	7
4	0·90	7
5	1·60	8
6	2·80	9
7	4·40	10
8	7·50	11

progressively shorter periods $[T(N_c) = 1/f_{co}]$ with decreasing magnitude and increasing source to station distance. This is caused by the recording and processing noise whose spectral amplitudes are shown (in Figure 1) by the lower shaded zone increasing from $FS \sim 10^{-1}$ in./sec (2.5×10^{-1} cm/sec) for $f \sim 10$ Hz to $FS \sim 1$ in./sec (2·5 cm/sec) near $f = 0{\cdot}1$ Hz.[41,59] At the high frequency end, the spectra are defined only up to 25 Hz, the high frequency limit chosen more for convenience in data processing than for poor signal to noise

ratio. Also, at high frequencies, the actual spectral amplitudes, as recorded by the strong motion accelerographs, have smaller amplitudes than those shown in Figure 1, because most strong motion transducers which contributed data to our data base had natural frequencies between 14–25 Hz.[30,60–62] While the algorithms for correction of the instrument response and for reconstruction of the ground motion can be extended to apply for frequencies higher than 25 Hz, so far we have not found it necessary to preserve the digitized data at a sampling rate higher than 50 points/sec.[41]

To show how it is possible to extend the spectral amplitudes to low and high frequencies, starting at the end periods of the spectra (the top shaded zone) shown in Figure 1 [$T(N_c)$ and 0·04 sec], for $T > T(N_c)$ and for $T < 1/25$ sec, the near-field spectra of strong motion acceleration, $FS_{NF}(\omega)$ [see equation (15)], is extrapolated to long periods by using equations whose functional form can be related to the earthquake source theory. This theory is used to determine only the shape of the spectra. The spectral amplitudes will be chosen so that the assumed spectra have the same amplitude as the empirically determined spectra [see equation (1)] at point $T(N_c)$. To describe the spectra for the far-field strong motion acceleration, $FS_{FF}(\omega) = \omega^2\Omega_{FF}(\omega)$ [see equation (26)], it is assumed that the shape of the Fourier spectral amplitudes can be described by functions which are similar to the body wave spectra in the Haskell[44] source model. The amplitudes of the extrapolated far-field spectra are determined by matching their amplitudes at $T(N_c)$ with the empirically determined spectra [equation (1)]. Finally, to present the spectral amplitudes for all distances [and for $T > T(N_c)$], a linear combination of the far-field and near-field spectra $[a_{FF}FS_{FF}(\omega) + a_{NF}FS_{NF}(\omega)]$ is considered with $a_{NF} + a_{FF} = 1$ for all distances. The quality of this approach is tested by comparing the extrapolated spectral amplitudes and their scaling parameters with independent measurements of various source and strong motion characteristics. Finally, for $f > 25$ Hz it is assumed that $FS(\omega) \sim A_Q e^{-k\omega/2}$, and it will be shown that the estimates of k for $5 < f < 25$ Hz can be used to extrapolate $FS(\omega)$ for $\omega > 50\pi$.

LOW FREQUENCY EXTENSION

Two separate cases are considered. In the first the recording site is so close to the earthquake source that the ground will experience permanent static displacement after an earthquake. This will occur when the site is close to the fault surface, typically at a distance smaller than the characteristic source dimension. This case is referred to as the 'near-field' ground motion. In the second case, it is assumed that the recording station is sufficiently far from the source so that the contributions from static displacement are negligible, i.e. all near and intermediate field terms[44] which attenuate as R^{-4} and R^{-2} have become negligible and only the body waves (attenuating like R^{-1}) and surface waves (attenuating like $R^{-1/2}$), where R is the epicentral distance, will contribute to the strong motion amplitudes.

Near-field displacements

Following Brune,[2] we represent the near-field displacement $d_{NF}(T)$ (Figure 2) by

$$d_{NF}(t) = d(1 - e^{-t/\tau}) \tag{8}$$

where d is the static displacement at the station following the earthquake. The real details of the ground motion are more complicated, but for the behaviour of the very long periods of the Fourier amplitude spectra of strong motion this may be a reasonable approximation. Obviously, equation (8) does not represent a forward solution for some assumed fault slip. It is an intuitive statement involving relevant parameters, and is used here to relate (e.g. via dimensional analysis) the permanent offset, d, and the measure of the time it takes to achieve it. When the observation point is on the fault surface, the average of d, $\bar{d}$, can be described by

$$\bar{d} = \frac{1}{2} C_0 \frac{\sigma r}{\mu} \tag{9}$$

where σ is the effective stress drop,[2] r is the equivalent (radius) dimension of the source area and μ is the rigidity in the source region (typically in the range from 1 to 4×10^{11} dyne/cm^2). C_0 is a 'constant' which depends on the type of faulting and is in the range from 0·4 to 1·6 (Table IV). The factor of 1/2 in equation (9) relates the displacement of a point (d) with an average source dislocation amplitude $\bar{u}$, which for symmetric

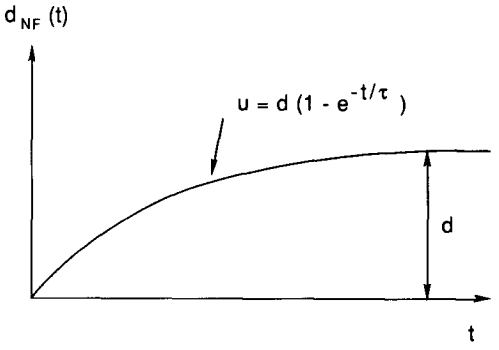

Figure 2. Near-field ground displacement d_{NF} versus time t

Table IV. $\bar{u} = C_0\sigma r/\mu$, $\bar{u} = 2\bar{d}$

Type of faulting and fault geometry[§]	C_0	r represents
Dip-slip displacement along an infinitely long narrow strip in a uniform shear field[63]	$3\pi/16$	Fault width
Infinitely long vertical surface fault with strike slip displacement[64]	$\pi^*/2-\pi^\dagger/4$	Fault width
Circular fault plane in an infinite medium[65]	$8^\ddagger/7\pi$	Diameter of circular dislocation (fault width)

* Surface fault.
† Deep fault.
‡ Poisson ratio, $\nu = 0{\cdot}25$.
§ To model the continuous changes of the faulting type and geometry, for the body of strong motion data studied here, $C_0^* = 0{\cdot}4, 0{\cdot}5, 0{\cdot}65, 0{\cdot}85, 1{\cdot}6$ and $1{\cdot}6$ for earthquake magnitudes $M = 3, 4, 5, 6, 7$ and 8, respectively. $C_0^* = 0{\cdot}4$ is representative of small circular faults, while $C_0^* = 1{\cdot}6$ represents long surface faults.

faulting is equal to $2\bar{d}$, and where the bars on u and d designate the average values taken over the fault surface. A vertical surface strike slip fault of length, L, and width, W, is considered which is equal to ξW_* ($0 \leqslant \xi \leqslant 1$, see Figure 3). W_* represents the fault width for faults which do not extend to the ground surface (when $\xi = 1$). We can represent the dislocation amplitudes by

$$u = u_{\max}\left(\frac{4x}{W_*} - \frac{4x^2}{W_*^2}\right)$$

Then the average dislocation is $\bar{u}(\xi) = (2\xi - \frac{4}{3}\xi^2)u_{\max}$. When $\xi = 1$ (buried fault) or when $\xi = 1/2$, $\bar{u} = \frac{2}{3}u_{\max}$. When $\xi = 3/4$, $\bar{u} = \frac{3}{4}u_{\max}$. On the ground surface, the dislocation amplitude ($2d$) and particle displacement (d) are described by

$$d = \frac{1-\xi}{\frac{1}{2} - \xi/3}\left(\frac{u_{\max}}{2}\right) \tag{10}$$

For $\xi \sim 0$, $d = \bar{u}$ and for $\xi = 1$, $d = 0$.

As the area of the fault surface (L is the fault length and $W = \xi W_*$ is the fault width), LW, increases with increasing magnitude, W becomes larger and so $u_{\max}$ is located at progressively greater depths.[66] Detailed source mechanism studies in California for the earthquakes which have contributed to the strong motion data base used here suggest that the largest dislocation amplitudes do not occur near the ground surface.[4,67–72] During the Parkfield earthquake of 1966, the dislocation occurred at depth[73] and its eventual

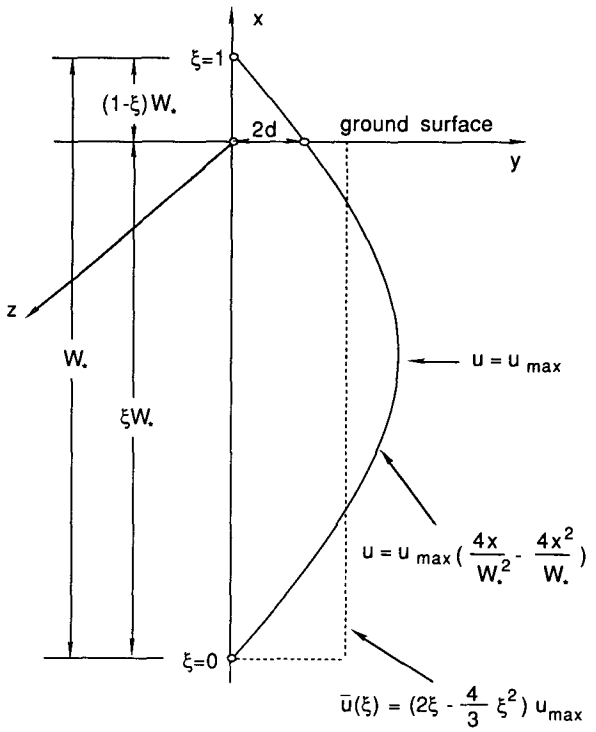

Figure 3. Dislocation amplitude (e.g. strike slip), u, on a vertical fault of width ξW_*, versus x (vertical axis with origin at the deepest point of a long fault of width ξW_*). $\bar{u}(\xi)$ represents the average dislocation, u_{max} is the maximum dislocation at $\xi = 0{\cdot}5$, and d is the maximum permanent displacement near the fault after the earthquake

surface expression grew through creep for about one year following the earthquake. For the purposes of this analysis, we need d (on the ground surface) and since the data are not available on the average displacement, $\bar{d}$, versus magnitude, faulting mechanisms, fault types and the distribution of rigidities and stresses on the two sides of the fault, we assume that the average of d occurs for $3/4 \leqslant \xi \leqslant 1$, and will approximate it by $\bar{d} \sim \frac{3}{4}\bar{u}/2$.

Estimates of the fault width, $W(= \xi W_*)$, versus magnitude suggest[74] growth of W versus magnitude, up to $W \sim 5$–20 km and $M \sim 6$. For larger magnitude events, W seems to become independent of magnitude. Correlations of the fault length, L and magnitude show large fluctuations. For $3 \leqslant M \leqslant 8$, most estimates tend to fall between

$$L_{\min} \approx 0{\cdot}01 \times 10^{0{\cdot}5M} \tag{11}$$

and

$$L_{\max} \approx 0{\cdot}2 \times 10^{0{\cdot}4M} \tag{12}$$

where L is measured in km.[66,75,76]

The Fourier amplitude spectrum of $d_{NF}(t)$ in equation (8) is

$$\Omega_{NF}(\omega) = \frac{d}{\tau\omega} \frac{1}{(\omega^2 + \tau^{-2})^{1/2}} \tag{13}$$

When $\omega \to 0$, $\Omega_{NF}(\omega) \to d/\omega$. Using the above approximate relationship between d and $\bar{u}$, this implies that

$$\bar{\Omega}_{\substack{NF \\ \omega \to 0}} \to \sim \frac{3}{8}\frac{\bar{u}}{\omega} \tag{14}$$

Fluctuations of d on the ground surface are considerable, and will depend on the relative position of the observation point with respect to the fault surface and the three-dimensional (3-D) character of the geologic medium surrounding the fault. Since we are dealing with empirical scaling of Fourier spectrum amplitudes, and because our model equation [equation (1)] represents the average trends for many observations, it will suffice for the purposes of this analysis to deal with the average trends of d as in the above equations.

For Fourier amplitude spectra of strong motion acceleration in the near field, $FS_{NF}(\omega)$, equation (13) gives

$$FS_{NF}(\omega) = \frac{\omega d}{[(\omega\tau)^2 + 1]^{1/2}} \tag{15}$$

where τ can be approximated by $\tau \sim r/\beta$, when $r < W/2$. When $L \gg W$, $\tau \approx L/v + T_0$, where v is the velocity with which the dislocation propagates along the fault length, and T_0 is the dislocation rise time.[44,46] For $L/v \gg T_0$, $\tau \to L/v$ and the corner frequency $f_1 = \omega_1/2\pi \to v/L$. For intermediate frequencies, $f_1 = (L/v + T_0)^{-1}$, with a typical value of $v = 2{\cdot}2$ km/sec, $T_0 \sim W/2\beta$ and $\beta \approx 3{\cdot}0$ km/sec. Here it may be assumed that, for typical strike slip faulting in California, the dislocation grows more or less as a circular dislocation up to $r \leqslant W/2$. When this size has been reached, we assume that the fault surface grows in terms of L only. Thus we can approximate $\omega\tau$ in equation (15) by

$$\omega\tau \approx \frac{2\pi}{T}\left(\frac{L}{2{\cdot}2} + \frac{W}{6}\right) \tag{16}$$

In equation (16), we choose $L = 0{\cdot}0133 \times 10^{0{\cdot}5M}$ which corresponds to L_{min}, already mentioned in equation (11). Why should we choose L_{min} rather than some average estimate of L? A detailed discussion of this question is beyond the scope of this paper, but it can be shown[66] that the data on L versus magnitude M, and the available data on the trends of strong motion amplitudes, suggest that L_{min} is the best choice.

For small intra-plate sources (e.g. $M < 4$), the fault length, L, and width, W, are about the same. For larger earthquakes, the fault continues to grow primarily and only through L, while W may only continue to increase slowly until it reaches the width of the seismogenic zone. A range of models describing W in terms of M has been considered.[66] This showed that the permissible variations of W versus magnitude are controlled well by the available data, and suggested a typical model with $W = L$ for $M < 3{\cdot}5$ and $W = 0{\cdot}1 \times 10^{0{\cdot}25M}$ for $M > 3{\cdot}5$. This dependence of W on magnitude is in good agreement with the data on the field estimates of W, and with the data on a corner frequency f_2, which is seen in the far-field spectra of shear waves,[53] and which can be approximated by $2{\cdot}2/W$.

By computing Fourier spectrum amplitudes for $T \to \infty$, we can evaluate the average dislocation $\bar{u}$ (cm) implied by the G4RM models and by the above choice of L and W. The result can be compared with other independent estimates of $\bar{u}$. For continuity with our previous studies,[36] and to focus on earthquakes which contributed to this data base, we use the data on $\bar{u}$, as shown in Figure 4. Each shaded region shows the fluctuations among $\bar{u}$ estimated from each of the G4RM. The three shaded regions are for probabilities $p(\varepsilon, T)$ of exceedance equal to 0·1, 0·5 and 0·9 (equation (7)). It is seen that the trends of $\bar{u}$ associated with the G4RM are in excellent agreement with our estimates of $\bar{u}$ using strong motion data, but are larger than the estimates of Thatcher and Hanks[77] which are based on distant recording and using body wave spectra.

Critical analysis of the accuracy of $\bar{u}$, estimated via different source mechanism studies, will reveal that considerable uncertainties and simplifications are required to obtain these results. Likewise, the above simple extrapolation of $FS(T \to \infty)$, using equation (15), to evaluate $FS(T)$ for $T > T(N_c)$ (see Table III) depends on the proper choice of $\omega\tau$ versus M (i.e. choice of L and W versus M). Yet, the agreement of the estimated $\bar{u}$ in this work with our previous estimates (Figure 4) suggests that the empirical spectral amplitudes of $FS(T)$ contain most of the relevant information, up to and including $T = T(N_c)$, to define the average $FS(T)$ for $T \gg T(N_c)$.

In $\tau = L/v + W/2\beta$, it is implicitly assumed that for $L \gg W$, τ is defined by a dislocation propagating from the focus at one end of the fault towards the other end of the fault, L_{min} and W_{min} km, unilaterally. Since it is the duration of faulting which is constrained by $\omega\tau$ and is fitted to the strong motion spectral amplitudes, it is seen that for bilateral faulting our scaling implies the fault length and width $L = 2L_{min}$. Thus, all field observations of fault length falling between L_{min} and $2L_{min}$ and W_{min} and $2W_{min}$ (Figure 5) would be in

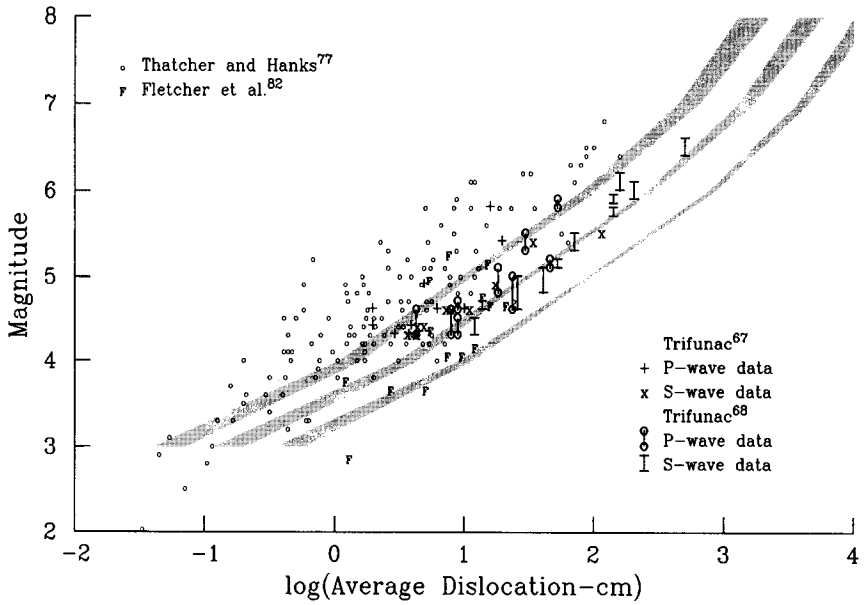

Figure 4. Magnitude versus average dislocation, $\bar{u}$, showing estimates of $\bar{u}$ from strong motion studeis[67, 68, 82] and from body wave spectra of distant recordings.[77] The three shaded zones represent $\bar{u}$ computed from the G4RM in this paper and for probabilities of exceedance $p(\varepsilon, T) = 0{\cdot}1, 0{\cdot}5$ and $0{\cdot}9$

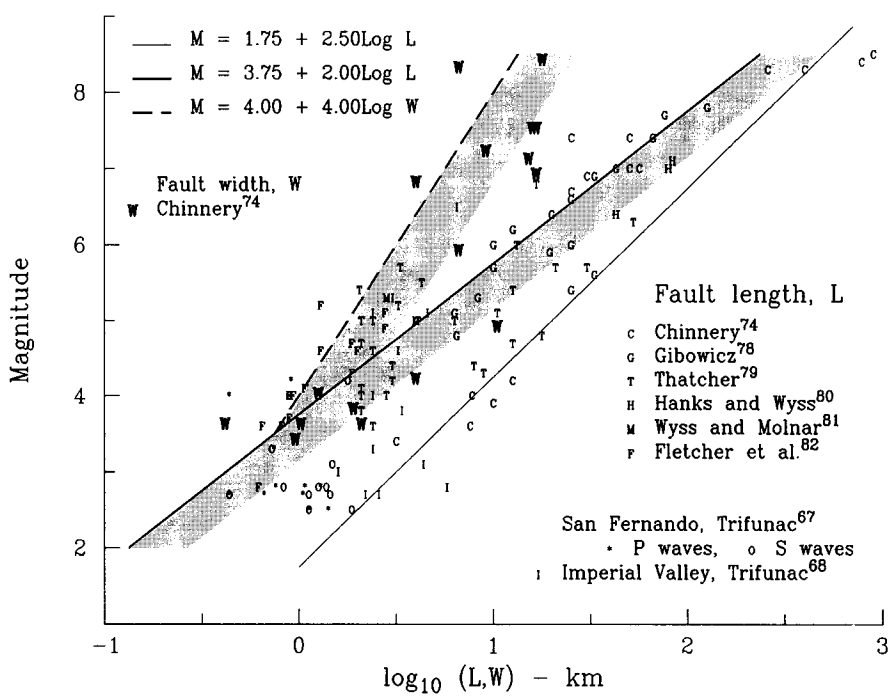

Figure 5. Summary of magnitude versus selected estimates of fault width, W and fault length, L.[67, 68, 74–82] The shaded areas are bounded by W_{min} and $2W_{min}$ and by L_{min} and $2L_{min}$

excellent agreement with our interpretation of near-field strong motion data. Detailed comparison of our estimates with the field and seismological estimates of fault length and width indicates excellent agreement.[66,74-81]

Far-field displacement.

As the observation point moves away from the source, the permanent offset (d) goes to zero and the ground displacement experiences only a 'transient pulse' which could be characterized by Brune's[2] pulse,

$$d_{FF}(t) \sim \frac{r}{R}\frac{\sigma\beta}{\mu} t' e^{-\alpha t'}, \quad t' \geqslant 0 \tag{17}$$

where $t' = t - R/B$ (r is the source dimension, σ the stress drop, β the shear wave velocity, R the source to station distance and μ the rigidity). The Fourier amplitude spectrum of d_{FF} in equation (17) is

$$\Omega_{FF}(\omega) = \frac{r}{R}\frac{\sigma\beta}{\mu}\frac{1}{\omega^2 + \alpha^2} \tag{18}$$

and the strong motion acceleration spectrum is

$$FS_{FF}(\omega) = \frac{r}{R}\frac{\sigma\beta}{\mu}\frac{1}{1 + (\alpha/\omega)^2} \tag{19}$$

Since $\alpha \approx 2{\cdot}34\beta/r$, and assuming that $r \sim L/2$ ($r = W/2$), for $\beta \approx 3$ km/sec, $\alpha/\omega \sim 2{\cdot}23T/L$. It is seen that as $T \to \infty$, equation (19) implies that $FS(T) \sim 1/T^2$. Also, since[65]

$$\underset{\omega \to 0}{\Omega_{NF}}(\omega) = M_0(4\pi\rho R\beta^3)^{-1} \tag{20}$$

$$\underset{T \to \infty}{FS_{FF}}(T) = \frac{\pi M_0}{\rho R\beta^3 T^2} \tag{21}$$

where $\rho = \mu/\beta^2$ and M_0 is the seismic moment defined by

$$M_0 = \mu\bar{u}A \tag{22}$$

and $\bar{u}$ is the dislocation amplitude ($u \sim 2d$) averaged over the fault surface A.

Equation (21), relating $FS_{FF}(\omega)$ and M_0 for long periods, T, and $FS_{FF}(\omega) \sim \sigma\beta/\mu$, for $\omega \gg \alpha$ [in equation (19)], has been used in numerous seismological studies considering the body wave spectra, mostly at teleseismic distances.[45,67,68,77,80,82] However, more detailed analyses[44,46,48,83] and observation[53] show that for intermediate and large earthquakes one corner frequency [α in equation (18)] cannot be used to explain the observed spectra and that at least two corner frequencies, $f_1 \sim 1/\tau$ and $f_2 \sim 1/W$, should be considered.[46,53,66,83] In this paper, two corner frequencies are used to model $FS_{FF}(\omega)$.

Using Haskell's[44] representation in the far-field for S waves, it is possible to compute the Fourier amplitude spectra of ground displacement if the dislocation function is specified on the fault surface. Assuming that this dislocation grows linearly during time T_0 until the final dislocation amplitude is reached, and propagates along the fault length L with constant velocity v, it can be shown that

$$|\Omega_{FF}| \sim \left|\frac{\sin \omega L/2v}{\omega L/2v}\right| \cdot \left|\frac{\sin \omega T_0/2}{\omega T_0/2}\right| \tag{23}$$

Equation (23) is characterized by two corner frequencies, one ($f_1 \sim (L/v)^{-1}$) associated with the duration of faulting and the other ($f_2 \sim 1/T_0$) with the duration of the dislocation rise time T_0. As $\omega \to \infty$, like equation (18), equation (23) implies $\Omega_{FF} \sim 1/\omega^2$.

For small earthquakes (e.g. $M < 4$–5, $\log_{10} M_0 \leqslant 23$, $\alpha \geqslant 2\pi$), f_1 and f_2 have similar values and it becomes difficult to distinguish between them experimentally. In those instances, the functional form of the Fourier amplitude spectra of strong motion acceleration, based on equation (19), is just as useful (for extrapolation to long periods) as the more detailed representation in equation (23) which will be used in this paper.

If one assumes a dislocation build-up function of the form $1 - \exp(-t/T_0)$, for $t > 0$, then[83]

$$|\Omega_{FF}| \sim \frac{\sin \omega L/2v}{\omega L/2v} \cdot \frac{1}{(1 + \omega^2 T_0^2)^{1/2}} \tag{24}$$

If it is assumed that the slip is controlled by its narrow dimension W, then the displacement rise time is $\sim W/2v$. Assuming then that this should roughly correspond to 90 per cent of the maximum dislocation[83] gives $2{\cdot}3T_0 = W/2v$ and the corner frequency

$$\omega_2 = 4{\cdot}6v/W \tag{25}$$

The other corner frequency $\omega_1 = 2\pi f_1$ depends on the duration of faulting L/v and on T_0.

Guided by the above results, Ω_{FF} was approximated by

$$\Omega_{FF}(T) = C_s \frac{1}{[1 + (W/2{\cdot}2T)^2]^{1/2}} \cdot \frac{1}{1 + \tau/T} \tag{26}$$

where constant C_s can be computed from

$$C_s = FS_{FF}(\omega_c)\omega_c^{-2}\left[1 + \left(\frac{W}{2{\cdot}2T}\right)^2\right]^{1/2}\left(1 + \frac{\tau}{T}\right) \tag{27}$$

with $\omega_c = 2\pi/T_c$ [$T_c = T(N_c)$, see Table IV] and $FS_{FF}(\omega_c)$ is the spectral amplitude computed from equation (1) (or its equivalent) for one of the four models (G4RM).

Equations (23), (24) and (27) result from a simplified consideration of the shear wave spectra only, while $FS(T)$ estimated from equation (1), via one of the G4RM, represents the Fourier amplitudes of the complete strong motion signal including all waves.

In our recent work, with the local magnitude scale computed from strong motion accelerograms,[42] M_L^{SM}, we found that the strong motion near the source leads to systematically larger estimates when compared with more distant seismological estimates of M_L. This difference, $D(\bar{M}_L^{SM}) = M_L^{SM} - M_p$ (where M_p stands for the published magnitude), for the strong motion data in the Western U.S. is summarized in Table V. It can be used to adjust the moment M_0^{SM}, computed from spectra of recorded strong ground motion, to agree with the moment M_0 computed from distant recordings

$$\log_{10} M_0 \approx \log_{10} M_0^{SM} - kD(\bar{M}_L^{SM}) \tag{28}$$

In equation (28), the factor k is the empirical slope[66,84] of $\log_{10} M_0$ versus M, and M_0^{SM} is the seismic moment computed from equations (20), (26) and (27) using the strong motion data in terms of the G4RM. $k = 1$ for $M < 4{\cdot}5$, $k = 1{\cdot}25$ for $4{\cdot}5 < M < 5$, $k = 1{\cdot}5$ for $5 < M < 7$ and $k = 1{\cdot}3$ for $M > 7$ were used in the present analysis. Equation (28) can then be used to evaluate M_0 and to compare it with other independent distant (> 200 km) estimates. This is shown in Figure 6, where the three shaded zones, for probabilities of exceedance equal to 0·1, 0·5 and 0·9, show $\log_{10} M_0$ versus magnitude.[66] The straight line given by $\log_{10} M_0 = 1{\cdot}5M_0 + 16$ and some data on field and seismic estimates of moment M_0 using body wave spectra and strong motion data are also shown. It is seen that the agreement between the estimates based on equation (28) and the results from the previous studies is very good.

To provide a continuous transition between $\Omega_{NF}(\omega)$ and $\Omega_{FF}(\omega)$, the results of Jovanovich *et al.*,[75,76] are used. They show that the error in representing the static displacement field by a point source is typically less than 5 per cent at distances greater than $4L$, where L is the source length. The distance S_1, between the station and the 'top' of the vertical fault with 'dimension' S [see equation (4)], at depth H, is defined as

$$S_1 = \begin{cases} [R^2 + (H - S)^2]^{1/2}, & H \geqslant S \\ R, & H < S \end{cases} \tag{29}$$

$S = 0{\cdot}01 \times 10^{0{\cdot}5M}$ is used when $S \leqslant 30$ km and $S = 30$ km for larger events, and then $FS_{NF}(T)$ and $FS_{FF}(T)$ are combined as follows.

$$FS(T) = FS_{NF}(T)e^{-(3s_1/4s)} + F_{FF}(T)(1 - e^{-(3s_1/4s)}), \quad T > T(N_c) \tag{30}$$

Table V*. $D(\bar{M}_L^{SM}) = \bar{M}_L^{SM\dagger} - M_p^{\ddagger}$ versus M_p

M_p	$D(\bar{M}_L^{SM})$
3·1	1·30
3·5	1·24
4·0	1·15
4·5	1·05
5·0	0·95
5·5	0·72
6·0	0·47
6·4	0·27
6·8	0·03
7·0	− 0·11
7·4	− 0·40
7·7	− 0·63
8·0	− 0·87

*From Reference 66.

†$\bar{M}_L^{SM}$, local magnitude estimated from computed response of Wood–Anderson seismograph excited by the recorded strong motion acceleration.

‡M_p is the published earthquake magnitude typically corresponding to M_L for $M_p \leqslant 6{\cdot}5$.

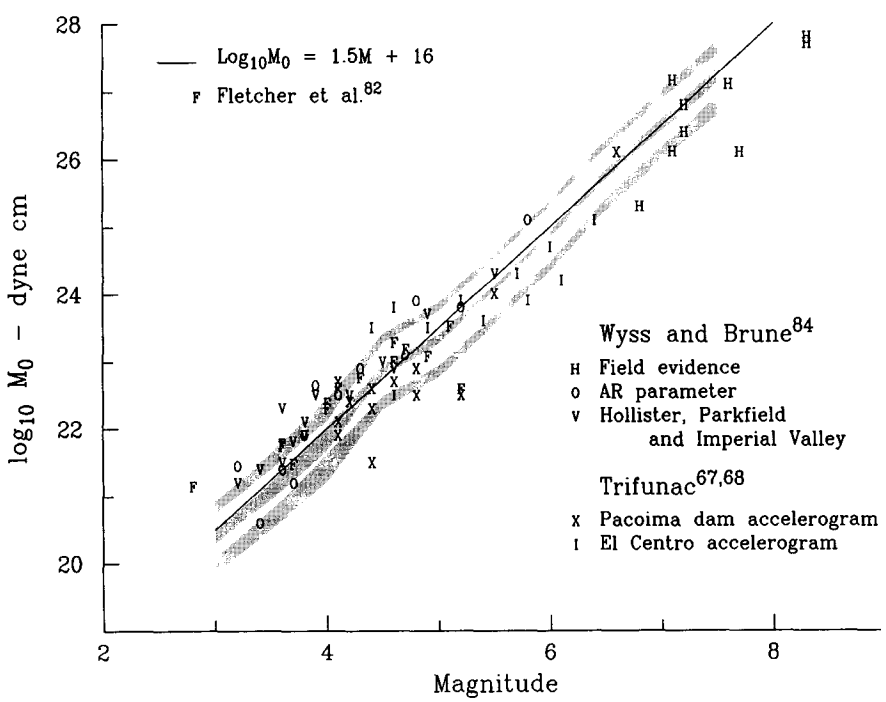

Figure 6. Seismic moment ($\log_{10} M_0$) versus magnitude. The three shaded zones illustrate fluctuations among different models from the G4RM and are for three probabilities of exceedance equal to 0·1, 0·5 and 0·9. For comparison, the empirical trend $\log_{10} M_0 = 1{\cdot}5M + 16$ and selected field data and data estimated from recordings (AR[84] and strong motion data[67,68,82]) are also shown

In the above expression, 3/4 is used to scale S_1/S so that when $S_1/S = 4$ the exponent is equal to 3, so that $e^{-3} \sim 0{\cdot}05$, in agreement with the recommendation of Jovanovich *et al.*[75,76] For $T < T(N_c)$ (see Table III) we use equations of the type illustrated by equation (1), depending on which of the G4RM is used.

FREQUENCIES NEAR THE MAXIMA OF $FS(T)$

The peaks of $FS(T)$ (Figure 1) occur near $T = 0{\cdot}1$ sec for $M = 3$ and move towards $T = 1$ sec for $M = 8$. The periods where the peaks occur also depend on the local site conditions and typically are longer for sites on 'softer' geological and/or soil deposits.

At the source ($\Delta = 0$), the effective stress is expected to become the main parameter which influences the high frequency spectral amplitudes, and for $f \geqslant 1/\tau$ and $f \geqslant 2{\cdot}2/W$ ($\omega > \alpha$) equations (13), (16) and (18) imply that $\Omega_{NF}(\omega) \approx \sigma\beta/\mu\omega^2$ and $\Omega_{FF}(\omega) \approx (r/R)\,(\sigma\beta/\mu\omega^2)$, respectively. In the absence of inelastic scattering and other possible high frequency attenuation mechanisms, this leads to constant acceleration spectra for $f > 1/\tau$ and $f \geqslant 2{\cdot}2/W$ ($\omega > \alpha$). It is the attenuation, approximated by $\exp(-\pi kf)$, where k is a coefficient to be discussed in the next section, that leads to the reduction of high frequency amplitudes, and so the 'peaks' in $FS(T)$ are observed. Assumng that $\exp(-\pi kf)$ becomes important only for $f > 1/\tau$ and $f > 2{\cdot}2/W$ ($\omega > \alpha$), the peak amplitudes of the acceleration spectra $FS(T)$ are proportional to $\sigma\beta/\mu$. From this, $\sigma \sim \mu FS(T = T_{peak})/\beta$ can be estimated. Taking $\mu \sim 1{\cdot}3 \times 10^6$ dyn/cm^2, $\beta \approx 3{\cdot}5$ km/sec (remembering that there are 2·54 cm per inch, and that 1 bar = 10^6 dyne/cm^2) gives $\sigma \sim FS(T = T_{peak})$ bars if $FS(T)$ is measured in (inch/sec).

This rough calculation can be used to compare the above results with the estimates of the stress drop from several source mechanism studies in the same area and for many of the earthquakes which contributed to our strong motion data base. This comparison is shown in Figure 7. It is seen that the overall agreement of the stress drop estimates is good. Trifunac[36] used a similar comparison with peak ground velocity. His results show more variation of σ with respect to magnitude. The three shaded areas in Figure 7, for $p = 0{\cdot}1, 0{\cdot}5$ and 0·9, and those computed for the G4RM show small changes of σ for $4 < M < 7$. This obviously results from the use of $\mathrm{Att}(\Delta, M, T)$ in the G4RM in this study rather than $\log_{10} A_0(R)$[57] (as used by Trifunac[36]), and because for the longer duration of shaking associated with larger magnitudes, the peak velocity will increase as $(\ln N)^{1/2}$, where N is the number of peaks in the velocity function. Most estimates of σ in Figure 7 have been derived on the basis of the Fourier amplitude spectra of shear waves and only a few employ the peak strong-motion velocity. In this study $FS(T)$ represents the Fourier amplitude spectrum of the complete strong motion record. It was concluded that the peak amplitudes of $FS(T)$ are not inconsistent with the previous estimates of σ.

The observed trends of the peaks of the Fourier amplitude spectra of strong motion acceleration ($\sim \sigma$) can be associated with a population of earthquakes which for $M \lesssim 5$ have essentially 'circular' faults ($W \sim L$) and are associated with one 'patch' (single event) dislocation[66] ($C_0^* \sim 0{\cdot}4$, see Table IV). Near this magnitude ($M = 5$), the width of the patch is believed to approach 3–5 km, and is constrained to grow further by the thickness of the seismogenic zone in California. For larger events, the larger fault area is realized by several ($M \sim 6$) or many such patches ($M \sim 8$, $C_0^* = 1{\cdot}6$). For $M > 5$, the expected amplitude of the stress drop grows linearly with $[\ln(WL/A_0)]^{1/2}$, where $A_0 \sim 16$ km^2, and the slope of this linear growth, $\bar{\sigma}$, corresponds to the root mean square amplitude of the peaks of the stress function on the fault, equal to ~ 100 bars.

HIGH FREQUENCY ATTENUATION

Little observational work has been done on high frequency ($f > 50$ Hz) attenuation of strong motion data.[66,85] Until recently, most of the recording instruments could register only moderately high frequencies (say < 30 Hz). To control the volume of strong motion data archives, routine processing of strong motion data has been performed up to 25 Hz (50 Hz sampling rate) even though the typical analog records are of good quality, so that we could extract even higher frequencies (perhaps up to 35 or 40 Hz, and with good accuracy[66]). The main obstacles in understanding the attenuation of high frequencies are the lack of data on the irregularities in the earth's crust and the relatively large distances separating the source and the strong

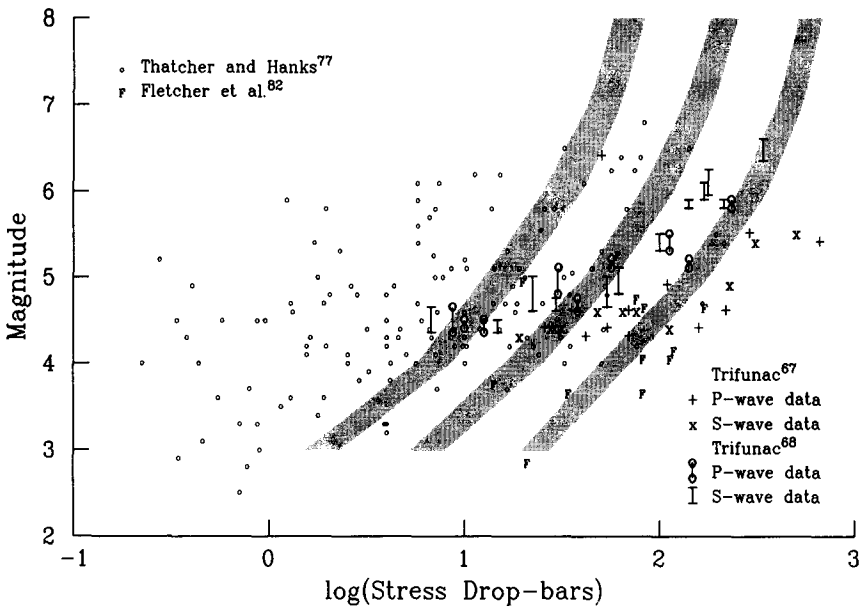

Figure 7. Magnitude versus stress drop (σ). The three shaded zones show the difference among the G4RM and have been plotted for $p(\varepsilon, T) = 0{\cdot}1, 0{\cdot}5$ and $0{\cdot}9$. For comparison, stress estimates from selected strong motion recordings[67,68,82] and distant body wave spectra[77] are shown

motion recording stations. Some areas could be saturated with broad band strong motion instruments, but it is not likely that we will be able to describe the 3-D inhomogeneities in the earth's crust for some time. Furthermore, the current computational capabilities to model scattering and diffraction for very high frequencies (short waves) are still very limited.[7,8] Thus, most investigators continue to use the empirical description for the combined effects of many possible attenuation mechanisms, including inelastic and scattering attenuations, in the form $\exp(-\omega\Delta/2Q\beta)$, where Δ is the distance travelled by the wave, Q is the quality factor and β is the (shear) wave velocity. For granites and basalts, Q is in the range of thousands, but for near-surface soil and sediments it can be as low as ten.

The high frequency spectral amplitudes[3] were approximated by $FS(f) = A_Q e^{-\pi k f}$. Using two frequencies f_1 and f_r, both larger than 10 Hz (say $f_1 = 25$ Hz and $f_r = 15{\cdot}4$ Hz), one can compute k and A_Q from

$$k = \frac{\ln FS(f_r) - \ln FS(f_1)}{\pi(f_1 - f_r)} \tag{31}$$

and

$$A_Q = FS(f_1)e^{\pi k f_1} \tag{32}$$

Then for $f > 25$ Hz ($T < 0{\cdot}04$ sec.)

$$FS(T) = A_Q e^{-\pi k/T} \tag{33}$$

can be used to extrapolate $FS(T)$ to high frequencies.[66]

The estimates of k for $15 < f < 25$ Hz and from G4RM are remarkably stable and in excellent agreement with several related studies of high frequency spectra of strong motion in California.[85] For $\Delta \sim 0$ km, k is between $0{\cdot}02$ and $0{\cdot}03$. It increases to about $0{\cdot}04$–$0{\cdot}05$ at $\Delta = 50$ km. From there, it grows slowly to $0{\cdot}055$–$0{\cdot}060$ at $\Delta = 200$ km. This implies that $Q \sim 10$, near the surface and for $\Delta = 0$, increasing to $Q \sim 300$ at $\Delta = 50$ km, and to $Q \sim 900$ at $\Delta = 200$ km, all in an essentially linear manner. For high frequency strong motions associated with body waves penetrating progressively greater depths as the epicentral distance increases, these trends are as one would expect them to be.[3,10,66,85]

Neither our empirical models of Fourier spectrum amplitudes (G4RM) nor the directly computed spectra of recorded strong motion indicate the existence of abrupt decay of the spectral amplitudes[66] in the sense of f_{max}.[50–52,85] If some low-pass filtering effects (sharper than $e^{-\pi kf}$) exist, they must occur for $f > 25$ Hz, i.e. outside the range for which strong motion data are processed and archived at present.

Assuming the simple functional form $Q = Q_0 f^{\gamma}$ to describe Q versus frequency f, our study leads to $\gamma \sim 0{\cdot}4$ (horizontal motions) and $\gamma \sim 0{\cdot}2$ (vertical motions) for frequencies between 5·3 and 9·1 Hz, and to $\gamma \sim 0{\cdot}7$ (horizontal motions) and $\gamma \sim 0{\cdot}6$ (vertical motions) for frequencies between 15·4 and 24 Hz and for distance range from 25 to 75 km. The seismological studies of the frequency-dependent Q (using Lg and coda waves) give $\gamma \sim 0{\cdot}1$–$0{\cdot}3$ for the central and south-eastern U.S., $\gamma \sim 0{\cdot}3$–$0{\cdot}4$ for north-eastern U.S. and $\gamma \sim 0{\cdot}4$–$0{\cdot}8$ for the western U.S.[66,85]

LOCAL SOIL AND GEOLOGICAL SITE CONDITIONS

At present, most empirical equations which describe the effects of local soil and geological site condition use factors [e.g. like the coefficient functions $b_2(T), b_4(T), b_7^{(1)}(T), b_7^{(2)}(T)$ in equation (1)] to describe the amplification of spectral amplitudes on 'soft' sites ($s = 0$ or $h > 0$ and $s_L = 1$ or 2) relative to 'hard', often referred to as 'rock', sites ($s = 2$ or $h = 0$ and $s_L = 0$). In equation (1), $b_2(T)$, for example, suggests a progressively larger factor to describe the local geological site effects since $b_2(T)$ is multiplied by h. However, other analyses suggest that it is not only the thickness of the layer that should be considered, but also the layer properties.[10] Furthermore, the frequency band within which such amplification occurs should depend on the characteristic dimensions of the inhomogeneities involved. To reconcile these requirements with the simplified average and overall effects as modelled by equations similar to equation (1), we will use here all the site amplification factors described in equation (1), but will modify the frequency range of their applicability, as follows.[10] Suppose that the average local amplification occurs only for the periods $T < T_1 = 4H_L/\beta_L$, where H_L and β_L are the thickness and the shear wave velocity in the equivalent layer describing the geological site conditions. It is further assumed that this amplification gradually dies out between $T_1 < T < 5T_1$. Figure 8 illustrates this by showing how spectral shapes change[10] for $T_1 = 16, 8, 4$ and 2 sec (assuming that $\beta_L = 1$ km/sec).

DISCUSSION AND CONCLUSIONS

This work is based on a simplified description of shear wave spectra as proposed by Brune.[2] This representation does not evolve from a solution of some specific source slip, but can be thought of as an intuitive collection of relevant parameters and functional relationships, which by observational understanding of the source mechanism and use of dimensional analysis result in a coherent picture of the main features of strong ground motion.[66] Consequently, our extrapolation of the Fourier amplitude spectra of strong ground motion into frequency bands beyond those which can be recorded by currently available strong motion accelerographs is likewise only intuitive and qualitative. Although an effort was made to make as many quantitative tests as possible, clearly we can only hope that real nature is not too different from these simplified average trends. Yet, the remarkable and encouraging outcome of this simple exercise is that the various comparisons of our model with the independent estimates of seismic moment, stress drop and average dislocation lead not only to good agreements, but also to resolution and scatter which are consistent with other independent estimates.[66]

The largest uncertainties in the present extrapolation are believed to exist near $T(N_c)$, where the empirical scaling models approach the recording and processing noise. The tests performed so far suggest that the resulting $FS(T)$ are very realistic for $3{\cdot}5 < M < 7$ and for horizontal ground motion. The slopes and amplitudes of empirically computed $FS(T)$ for vertical motions suggest that near $T = T(N_c)$ our empirical models may not be reliable for $M > 6{\cdot}5$. To understand these amplitudes we need more recorded accelerograms for $M > 7$, and so we must patiently wait for this data to become available.

Extrapolation of $FS(T)$ on a log–log scale by equation (15) from $T(N_c)$ (or from T_1) towards $T \to \infty$ sec (and $5T_1$) appears reasonable and agrees favourably with the known trends of seismic moment M_0 and of the

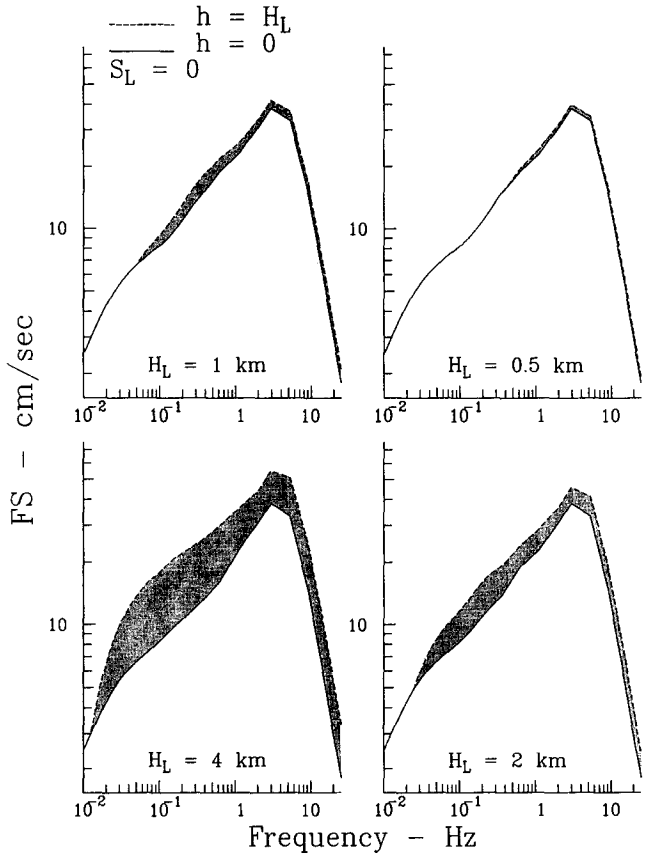

Figure 8. Examples of how the spectral amplitudes (broked lines) amplified by the local geologic conditions (depth of sediments, h) depend on the thickness of the sedimentary layer $h = H_L$. The solid lines show $FS(T)$ for $H_L = 0$

average dislocation amplitudes, $\bar{u}$, versus earthquake magnitude. Since the corner frequencies, $f_1 = 1/\tau$ and $f_2 = 2{\cdot}2/W$, in the near-field ground motion are $\sim v/r$, where v is the dislocation velocity (typically between 2 and 3 km/sec) and r is the representative source dimension (L and W), it is seen that τ can be larger than $T(N_c)$. This is so assuming that for the frequencies considered here rupture occurs as a 'smooth' process. Many studies have suggested that the fault slips irregularly, with large dislocations distributed at several or many 'hot' spots with large dislocation amplitudes, making larger events look like a sequence of smaller events. While this faulting behaviour can affect τ appreciably, at present relaible data are not available to introduce and verify such behaviour in this analysis.

For similarity to exist among different earthquake events, the following must be satisfied: (1) W/L = constant, (2) $\bar{u}/W$ = constant and (3) v/β = constant. For earthquakes occurring in different tectonic environments, including both intra-plate and inter-plate events, several investigators have concluded that the similarity hypothesis could be accepted for large earthquakes.[49] In earthquake engineering applications, one is interested in the similarity aspect in a more local and regional sense, to the extent that it may influence the estimation of strong shaking from sources typically not further than 200–300 km from the site. Unless one is dealing with a site where both a large subduction zone (e.g. the coast of Alaska, or the east coast of Japan) and the local shallow thrust and strike slip faults contribute to the seismic risk, it may be appropriate to consider only a more restricted set of events, for example the thrust and strike slip faults in southern California. In this paper only such events are considered because all the strong motion data used to develop the G4RM were recorded in this area. The present data and models are consistent with more or less 'circular' faults for M smaller that about 4 ($C_0^* \sim 0{\cdot}4$), gradually changing to thrust and dip-slip faulting as L and

$W \rightarrow$ 5–10 km, and as L begins to exceed W. Then, as W becomes constrained by the width of the seismogenic zone, our typical event 'looks' like a strike-slip fault ($C_0^* \sim 1{\cdot}6$). This leads to continuous changes of C_0^* from 0·4 to 1·6 (see Table IV), and thus implies that the similarity requirement expressed via W is not satisfied.[66]

The highly 'local' nature of strong motion recording (local in the sense of the proximity to the fault, say less than 100 km), and the fact that it is $\bar{u}$ and not the overall source magnitude or moment and long source dimensions (L) which govern the near-field strong motion amplitudes, all agree with the observed trends of strong motion amplitudes predicted by the G4RM.

Numerous further tests and studies of the relationships analogous to equations (15), (26), (30), and (33) (and of the associated amplitudes, corner frequencies and scaling parameters) are possible. Also the empirical equations exemplified by equation (1) can be used to investigate the high frequency attenuation and the trends implied by the peaks of spectral amplitudes for frequencies less than 25 Hz. Many of these studies have been completed[66] in the process of selecting and verifying the equations which are presented here, but their presentation is far beyond the scope of this paper. The picture which emerges from this work is that of detailed internal consistency and of excellent agreement with near strong ground motion and distant seismological inferences on the one hand, and with the simplified source representations (based on dimensional analysis) on the other.

ACKNOWLEDGEMENTS

This work has been supported in part by the California Department of Transportation and the City and County of Los Angeles, through the Southern California Earthquake Center. This support is gratefully acknowledged.

APPENDIX: NOTATION

$\mathscr{A}_0(T)$ parabola w.r.t. $\log_{10} T$ which defines the frequency-dependent attenuation in $\Delta^{\mathscr{A}_0(T)}$ (see equation (2)),

$$\mathscr{A}_0(T) = \begin{cases} -0{\cdot}732 & T \geqslant 1{\cdot}8 \text{ sec} \\ a + b \log_{10} T + C(\log_{10} T)^2 & T < 1{\cdot}8 \text{ sec} \end{cases}$$

where $a = -0{\cdot}767$, $b = 0{\cdot}271$ and $c = -0{\cdot}526$ (see Reference 58)

$\text{Att}(\Delta, M, T)$ a function describing the frequency dependent ($f = 1/T$) attenuation of the spectral amplitudes versus distance Δ and magnitude M (is defined by equation (2))

a_{NF}, a_{FF} a function describing the contribution of near-field ($a_{NF} = e^{-3S_1/4S}$) and of far-field spectra ($a_{FF} = 1 - e^{-3S_1/4S}$) to the Fourier amplitude spectra of strong motion acceleration, $FS(T)$

A fault area, $A = WL$ (km^2)

A_0 area of a single patch (asperity)

A_Q zero frequency asymptote in $FS(f) = A_Q e^{-\pi k f}$

$b_i(T)$ empirical scaling 'coefficients' in equation (1)

$b_i^{(j)}(T)$ empirical scaling coefficients in equation (1) for the indicator variable j

C_0 scaling 'coefficient' relating the average fault displacement, $\bar{d}$, or the average fault dislocation, $\bar{u}$ ($\bar{u} = 2\bar{d}$), with the source dimension r and the rigidity of the surrounding rocks, μ

C_0^* proposed 'average' trend of C_0 versus M

C_s a scaling constant [see equations (26) and (27)]

d permanent ground displacement, $d = d_{NF}(t)$, for $t \rightarrow \infty$

$d(t)$ displacement of the ground motion versus time

$d_{NF}(t)$ near-field strong motion displacement (for $\Delta < S$)

$d_{FF}(t)$ far-field strong motion displacement (for $\Delta \gg S$)

$\bar{d}$	average of $d_{NF}(t)$, for $t \to \infty$, on the fault surface
$D(\bar{M}_L^{SM})$	difference between M_L^{SM} and M_p
f	frequency (Hz)
f_1	corner frequency, $f_1 = (L/v + T_0)^{-1}$ (Hz)
f_2	corner frequency, $f_2 = 2{\cdot}2/W$ (Hz)
f_p	frequency where $FS(f)$ has peak amplitude (see Figure 1)
f_{co}	frequency [$= 1/T(N_c)$] below which equation (1) is not valid (see Table II)
f_{max}	high frequency corner or cut-off frequency[52]
$FS(T), FS(\omega), FS(f)$	Fourier amplitude spectrum of strong motion acceleration at period T, circular frequency ω, or frequency f
$FS_{NF}(w)\, FS_{NF}(T)$, $FS_{FF}(w), FS_{FF}(T)$	Fourier amplitude spectra of near-field and far-field strong motion acceleration, at frequency ω, or period T
G4RM	group of four regression models. Model 4 is shown in equation (1). (1. MAG-SITE;[58] 2. MAG-DEPTH;[58] 3. MAG-SITE-SOIL;[55] 4. MAG-DEPTH-SOIL[54])
h	depth (thickness) of the sedimentary layer beneath the station (km)
H	focal depth (km)
H_L	thickness of a horizontal sedimentary layer over elastic half space, $h = H_L$ for a horizontal layer with constant thickness
k	slope of $\log_{10} M_0$ versus M [see equation (28)]
L, L_{min}, L_{max}	fault length, minimum fault length and maximum fault length (km)
M	magnitude
M_{min}, M_{max}	minimum and maximum magnitudes defining the range $M_{min} < M < M_{max}$, where the strong motion amplitudes begin to saturate. For $M > M_{max}$, $FS(T)$ in equation (1) is constant, i.e. does not grow with M
M_0	seismic moment ($= \mu \bar{u} A$) (dyne cm)
M_0^{SM}	seismic moment computed from strong motion data
M_L	the local magnitude scale[57]
M_L^{SM}	local magnitude computed from strong motion accelerograms[42]
M_p	'magnitude' as published in various catalogues (without specification of the wave type used, or the procedure employed)
N_p	number of peaks of a random function ($N_p = WL/A_0$)
$p(\varepsilon, T)$	probability density function describing the distribution of $\varepsilon(T)$ in equation (7)
Q	the quality factor
Q_0	the value of Q at $f = 1$ Hz
r	the characteristic source dimension (see Table IV) (km)
R	epicentral distance (km)
R_0	transition distance where the frequency dependent attenuation $\mathrm{Att}(\Delta, M, T)$ becomes $\sim R/200$ as in $\log_{10} A_0(R)$[57]
s	the geologic site condition parameter ($s = 0$ for sediments, $s = 2$ for basement rock and $s = 1$ for intermediate sites)
s_L	a parameter describing the local soil site condition ($s_L = 0$ for 'rock' sites, $s_L = 1$ stiff sites and $s_L = 2$ for deep soil sites)
S	the source dimension used in equation (3) and defined by equation (4). Also used in equation (29), the "source dimension" $S = 0{\cdot}01 \times 10^{0{\cdot}5M}$ (km)
$S_L^{(1)}, S_L^{(2)}$	indicator variables describing the local soil conditions [see equation (5)]
S_0	the coherence radius[49] of the source (km)
S_1	distance between the station and the top of a vertical fault (km)
t	time (sec)
t'	delayed time, $t' = t - R/\beta$
T	period of vibration, $T = 1/f$ (sec)

$T(N)$	periods ($N = 1,2,\ldots,12$) for which $b_i(T)$, M_{min}, M_{max}, $\mu(T)$ and $\sigma(T)$ are prescribed in Table I. Equation (1) can be used for $N < N_c$ (see Table II) i.e. for $T < T(N_c)$
T_1	the first interference period $T_1 = 4H_L/\beta_L$, for a horizontal layer of thickness H_L and with shear wave velocity β_L
T_p	period where $FS(T)$ is maximum, $T_p = 1/f_p$
T_c	cut off period $T_c = T(N_c) = 1/f_{co}$ (see Table II)
T_0	the dislocation rise time, $T_0 \sim \bar{u}\mu/\sigma\beta$ (sec)
u, u_{max}	dislocation amplitude, maximum dislocation amplitude
$\bar{u}$	dislocation averaged over the fault surface
v	dislocation velocity (km/sec)
W, W_{min}, W_*	fault width, minimum fault width, a distance such that $W = \xi W_*$, for $0 < \xi < 1$ (km)
α	corner frequency in Brune's spectrum[2] [see equation (18)]
β	velocity of shear waves, $\beta = (\mu/\rho)^{1/2}$ (km/sec)
γ	exponent in $Q = Q_0 f^\gamma$
Δ	the representative source to station distance [see equation (3)]
$\varepsilon(T)$	residuals, $\varepsilon(T) = \log_{10} FS(T) - \log_{10} \widehat{FS}(T)$ [see equation (6)]
k	the high frequency attenuation constant, $k = \Delta/(Q\beta)$
μ	shear modulus, $\mu = \rho\beta^2$ (dyne/cm^2)
$\mu(T)$	the mean of distribution $p(\varepsilon, T)$ in equation (7)
ν	an indicator variable, $\nu = 0$ for horizontal motion, $\nu = 1$ for vertical motion
π	constant ($= 3{\cdot}14159$)
ρ	material density (g/cm^3)
σ	effective stress (also used as stress drop[2]) defined as the difference of stress before the earthquake and the frictional stress during faulting[2]
$\bar{\sigma}$	root-mean-square of the peak stress amplitudes on the fault surface
$\sigma(T)$	standard deviations of the distribution $p(\varepsilon, T)$ in equation (7)
τ	the characteristic source time, $\tau = 1/f_1 = L/v + T_0$
ω	circular frequency, $\omega = 2\pi f$ (rad/sec)
$\Omega_{NF}(\omega), \Omega_{FF}(\omega)$	near-field and far-field Fourier amplitude spectra of strong motion displacement
ω_1, ω_2	corner frequencies $\omega_1 = 2\pi f_1$, $\omega_2 = 2\pi f_2$ (rad/sec)
ω_c	cut-off frequency, $\omega_c = 2\pi f_c$ (rad/sec)

REFERENCES

1. D. E. Hudson, 'Some problems in the application of spectrum techniques to strong-motion earthquake analysis', *Bull. seism. soc. Am.* **52**, 417–430 (1962).
2. J. N. Brune, 'Tectonic stress and the spectra of seismic shear waves', *J. geophys. res.* **75**, 4997–5009 (1970).
3. M. D. Trifunac, 'Analysis of strong earthquake ground motion for prediction of response spectra', *Earthquake eng. struct. dyn.* **2**, 59–69 (1973).
4. M. D. Trifunac, 'A three-dimensional dislocation model for the San Fernando, California, earthquake of February 9, 1971', *Bull. seism. soc. Am.* **64**, 149–172 (1974).
5. N. Moeen-Vaziri and M. D. Trifunac, 'Scattering and diffraction of plane SH-waves by two-dimensional inhomogeneities', *Soil dyn. earthquake eng.* **7**, 179–188 (1988).
6. N. Moeen-Vaziri and M. D. Trifunac, 'Scattering and diffraction of plane P- and SV-waves by two-dimensional inhomogeneities', *Soil dyn. earthquake eng.* **7**, 189–200 (1988).
7. M. Todorovska and V. W. Lee, 'A note on response of shallow circular valleys to Rayleigh waves: analytical approach', *Earthquake eng. eng. vib.* **10**, 21–34 (1990).
8. M. Todorovska and V. W. Lee, 'Surface motion of circular alluvial valleys of variable depth for incident plane SH waves', *Soil dyn. earthquake eng.* **10**, 192–200 (1991).
9. H. B. Seed, C. Ugas and J. Lysmer, 'Site dependent spectra for earthquake resistant design', *Bull. seism. soc. Am.* **66**, 221–243 (1976).
10. M. D. Trifunac, 'How to model amplification of strong earthquake motions by local soil and geologic site conditions', *Earthquake eng. struct. dyn.* **19**, 833–846 (1990).
11. H. Cao and V. W. Lee, 'Scattering and diffraction of plane P-waves by circular cylindrical canyons with variable depth-to-width ratio', *Soil dyn. earthquake eng.* **9**, 141–150 (1990).

12. V. W. Lee and H. Cao, 'Diffraction of SV waves by circular canyons of various depths', *J. eng. mech. ASCE* **115**, 2035–2056 (1989).
13. M. D. Trifunac, 'Surface motion of a semi-cylindrical alluvial valley for incident plane SH waves', *Bull. seism. soc. Am.* **61**, 1755–1770 (1971).
14. J. E. Luco, 'Linear soil–structure interaction: a review, earthquake ground motion and its effects on structures', *AMD-53*, ASME, New York, pp. 41–57, 1982.
15. M. I. Todorovska and M. D. Trifunac, 'Radiation damping during two-dimensional building–soil interaction', *Report No. 91-01*, Department of Civil Engineering, University of Southern California, Los Angeles, CA, (1991).
16. M. I. Todorovska and M. D. Trifunac, 'The system damping, the system frequency and the system response peak amplitudes during in-plane building–soil interaction', *Earthquake eng. stuct. dyn.* **21**, 127–144 (1992).
17. F. E. Udwadia and M. D. Trifunac, 'Characterization of response spectra through the statistics of oscillator response', *Bull. seism. soc. Am.* **64**, 205–219 (1974).
18. I. D. Gupta and M. D. Trifunac, 'A note on contribution of torsional excitation to earthquake response of simple symmetric buildings', *Earthquake eng. eng. vib.* **7**, 27–46 (1987).
19. I. D. Gupta and M. D. Trifunac, 'Order statistics of peaks of response to multi-component seismic excitation', *Bull. Ind. soc. earthquake tech.* **24**, 135–159 (1987).
20. I. D. Gupta amd M. D. Trifunac, 'A note on contribution of rocking excitation to earthquake response of simple buildings', *Bull. Ind. soc. earthquake tech.* **25**, 73–89 (1988).
21. I. D. Gupta and M. D. Trifunac, 'Order statistics of peaks in earthquake response', *J. eng. mech. ASCE EMD: Engineering Mechanics Division* **114**, 1605–1627 (1988).
22. V. K. Gupta and M. D. Trifunac, 'Response of multistoried buildings to ground translation and rocking during earthquakes', *J. probabilistic eng. mech.* **5**, 138–145 (1990).
23. V. K. Gupta and M. D. Trifunac, 'A note on contributions of ground torsion to seismic response of symmetric multistoried buildings', *Earthquake eng. eng. vib.* **10**, 27–40 (1990).
24. V. K. Gupta and M. D. Trifunac, 'Response of multistoried buildings to ground translation and torsion during earthquakes', *Eur. earthquake eng.* **1**, 34–42 (1990).
25. V. K. Gupta and M. D. Trifunac, 'Seismic response of multistoried buildings including the effects of soil structure interaction', *Soil dyn. earthquake eng.* **10**, 414–422 (1991).
26. V. K. Gupta and M. D. Trifunac, 'Effect of ground rocking on dynamic response of multistoried building during earthquakes', *Struct. eng./earthquake eng. JSCE* **8**, 43–50 (1991).
27. J. G. Anderson and M. D. Trifunac, 'Uniform risk functionals for characterization of strong earthquake ground motion', *Report No. 77-02*, Department of Civil Engineering, University of Southern California, Los Angeles, CA, 1977.
28. J. G. Anderson and M. D. Trifunac, 'Uniform risk functionals for characterization of strong earthquake ground motion', *Bull. seism. soc. Am.* **68**, 205–218 (1978).
29. M. D. Trifunac and M. I. Todorovska, 'Methodology for selection of earthquake design motions for important engineering structures', *Report No. 89-01*, Department of Civil Engineering, University of Southern California, Los Angeles, CA, 1989.
30. V. W. Lee, A. Amini and M. D. Trifunac, 'Noise in earthquake accelerograms', *J. eng. mech. div. ASCE* **108**, 1121–1129 (1982).
31. V. W. Lee and M. D. Trifunac, 'EQUINFOS (the strong-motion earthquake data information system)', *Report No. 82-01*, Department of Civil Engineering, University of Southern California, Los Angeles, CA, 1982.
32. V. W. Lee and M. D. Trifunac, 'Strong earthquake ground motion data in EQUINFOS: Part I', *Report No. 87-01*, Department of Civil Engineering, University of Southern California, Los Angeles, CA, 1987.
33. L. R. Jordanovski, V. W. Lee, M. Manić, T. Olumčeva, C. Sinadinovski, M. Todorovska and M. D. Trifunac, 'Strong earthquake ground motion data in EQINFOS: YUGOSLAVIA, Part I', *Report No. 87-05*, Department of Civil Engineering, University of Southern California, Los Angeles, CA, 1987.
34. G. Georgiev, I. Paskaleva, V. W. Lee and M. D. Trifunac, 'Strong earthquake ground motion data in EQINFOS: accelerograms recorded in Bulgaria between 1981 and 1987', Bulgarian Academy of Sciences, CLSMEE, Sofia 1990; also Department of Civil Engineering, *Report No. 90-02*, University of Southern California, Los Angeles, CA, 1990.
35. M. D. Trifunac, 'Preliminary empirical model for scaling Fourier amplitude spectra of strong ground acceleration in terms of earthquake magnitude, source to station distance and recording site conditions', *Bull. seism. soc. Am.* **66**, 1343–1373 (1976).
36. M. D. Trifunac, 'Preliminary analysis of the peaks of strong earthquake ground motion—dependence of peaks on earthquake magnitude, epicentral distance and the recording site conditions', *Bull. seism. soc. Am.* **66**, 189–219 (1976).
37. M. D. Trifunac and V. W. Lee, 'Preliminary empirical model for scaling Fourier amplitude spectra of strong ground acceleration in terms of earthquake magnitude source to station distance, site intensity and recording site conditions', *Report No. 85-03*, Department of Civil Engineering, University of Southern California, Los Angeles, CA, 1985.
38. M. D. Trifunac and V. W. Lee, 'Direct empirical scaling of response spectral amplitudes from various site and earthquake parameters', *Report NUREG/CR-4903*, Vol. 1, U.S. Nuclear Regulatory Commission, 1987.
39. M. D. Trifunac and V. W. Lee, 'Frequency dependent attenuation of strong earthquake ground motion', *Soil dyn. earthquake eng.* **9**, 3–15 (1990).
40. A. Amini and M. D. Trifunac, 'Optimum frequency and damping for optically recording strong motion accelerograms', *Soil dyn. earthquake eng.* **1**, 189–194 (1982).
41. V. W. Lee and M. D. Trifunac, 'Automatic digitization and processing of accelerograms using PC', *Report No. 90-03*, Department of Civil engineering, University of Southern California, Los Angeles, CA, 1990.
42. M. D. Trifunac, 'M_L^{SM}', *Soil dyn. earthquake eng.* **10**, 17–25 (1991).
43. V. W. Lee, 'A note on computed magnitude M_L^{SM} from strong motion records', *Soil dyn. earthquake eng.* **10**, 10–16 (1991).
44. N. A. Haskell, 'Elastic displacement in the near field of a propagating fault', *Bull. seism. soc. Am.* **59**, 965–980 (1969).
45. D. M. Boore, 'Stochastic simulation of high-frequency ground motions based on seismological models of the radiated spectra', *Bull. seism. soc. Am.* **73**, 1865—1894 (1983).
46. W. B. Joyner, 'A scaling law for the spectra of larger earthquakes', *Bull. seism. soc. Am.* **74**, 1167–1188 (1984).
47. K. Aki, 'Scaling law of seismic spectrum', *J. geophys. res.* **72**, 1217–1231 (1967).

48. J. Boatwright, 'The seismic radiation from composite models of faulting', *Bull. seism. soc. Am.* **78**, 489–508 (1988).
49. A. A. Gusev, 'Descriptive statistical model of earthquake source radiation and its application to an estimation of short-period strong motion', *Geophys. j. royal astr. soc.* **74**, 787–808 (1983).
50. A. S. Papageorgiou and K. Aki, 'A specific barrier model for the quantitative description of inhomogeneous faulting and the prediction of strong ground motion. I. Description of the model', *Bull. seism. soc. Am.* **73**, 693–722 (1983).
51. A. S. Papageorgiou and K. Aki, 'Scaling law of far-field spectra based on observed parameters of the specific barrier model', *Pageoph* **123**, 353–374 (1985).
52. T. C. Hanks, 'f_{max}', *Bull. seism. soc. Am.* **72**, 1867–1879 (1982).
53. A. S. Papageorgiou, 'On two characteristic frequencies of acceleration spectra: patch corner frequency and f_{max}', *Bull. seism. soc. Am.* **78**, 509–529 (1988).
54. M. D. Trifunac, 'Dependence of Fourier spectrum amplitudes of recorded strong earthquake accelerations on magnitude, local soil conditions and on depth of sediments', *Earthquake eng. struct. dyn.* **18**, 999–1016 (1989).
55. M. D. Trifunac, 'Empirical scaling of Fourier spectrum amplitudes of recorded strong earthquake accelerations in terms of magnitude and local soil and geologic conditions', *Earthquake eng. eng. vib.* **9**, 23–44 (1989).
56. M. D. Trifunac and A. G. Brady, 'On the correlation of seismic intensity scales with the peaks of recorded strong ground motion', *Bull. seism. soc. Am.* **65**, 139–162 (1975).
57. C. F. Richter, *Elementary Seismology*, Freeman, San Francisco, CA, 1958.
58. M. D. Trifunac and V. W. Lee, 'Empirical models for scaling Fourier amplitude spectra of strong ground acceleration in terms of earthquake magnitude, source to station distance, site intensity and recording site conditions', *Soil dyn. earthquake eng.* **8**, 110–125 (1989).
59. V. W. Lee, M. D. Trifunac and A. Amini, 'Noise in earthquake accelerograms', *J. eng. mech. div. ASCE* **108**, 1121–1129 (1989).
60. M. D. Trifunac and D. E. Hudson, 'Laboratory evaluation and instrument corrections of strong motion accelerographs', *EERL 70-04*, Earthquake Engineering Research Laboratory, California Institute of Technology, Pasadena, CA, 1970.
61. M. D. Trifunac, 'Zero baseline correction of strong-motion accelerograms', *Bull. seism. soc. Am.* **61**, 1201–1211 (1971).
62. M. D. Trifunac, 'A note on correction of strong-motion accelerograms for instrument response', *Bull. seism. soc. Am.* **62**, 401–409 (1972).
63. A. T. Star, 'Slip in a crystal and rupture in a solid due to shear', *Cambridge philos. soc. proc.* **24**, 489–500 (1928).
64. L. Knopoff, 'Energy release in earthquakes', *Geophys. j.* **1**, 44–52 (1958).
65. V. I. Keilis-Borok, 'On estimation of the displacement in an earthquake source and of source dimensions, *Annali Geofizica* **12**, 205–214 (1959).
66. M. D. Trifunac, 'Broad band extension of Fourier amplitude spectra of strong motion acceleration, *Rep. No. CE 93-01*, Department of Civil Engineering, University of Southern California, Los Angeles, CA, 1993.
67. M. D. Trifunac, 'Stress estimates for San Fernando, California earthquake of February 9, 1971: main event and thirteen after shocks', *Bull. seism. soc. Am.* **62**, 721–750 (1972).
68. M. D. Trifunac, 'Tectonic stress and source mechanism of the Imperial Valley, California earthquake of 1940', *Bull. seism. soc. Am.* **62**, 1283–1302 (1972).
69. R. J. Archuleta, 'Analysis of near-source static and dynamic measurement from the 1979 Imperial valley earthquake', *Bull. seism. soc. Am.* **72**, 1927–1956 (1982).
70. S. Hartzell and T. Heaton, 'Inversion of strong ground motion and teleseismic wave form data for the fault rupture history of the 1979 Imperial valley, California earthquake', *Bull. seism. soc. Am.* **73**, 1553–1584 (1983).
71. S. Hartzell and D. Helmberger, 'Strong-motion modeling of the Imperial valley earthquake of 1979', *Bull. seism. soc. Am.* **72**, 571–596 (1982).
72. A. Olson and R. Apsel, 'Finite faults and inverse theory with applications to the 1979 Imperial valley earthquake', *Bull. seism. soc. Am.* **72**, 1969–2002 (1982).
73. M. D. Trifunac and F. E. Udwadia, 'Parkfield, California, earthquake of June 27, 1966: a three-dimensional moving dislocation', *Bull. seism. soc. Am.* **64**, 511–533 (1974).
74. M. A. Chinnery, 'Earthquake magnitude and source parameters', *Bull. seism. soc. Am.* **59**, 1969–1982 (1969).
75. D. Jovanovich, M. I. Husseini and M. A. Chinnery, 'Elastic dislocations in a layered half space—I. Basic theory and numerical methods', *Geophys. j. roy. astron. soc.* **39**, 205–217 (1974).
76. D. Jovanovich, M. I. Husseini and M. A. Chinnery, 'Elastic dislocation in a layered half space—II. Point source', *Geophys. j. roy. astron. soc.* **39**, 219–239 (1974).
77. W. Thatcher and T. C. Hanks, 'Source parameters of Southern California earthquakes', *J. geophys. res.* **78**, 8547–8576, (1973).
78. S. T. Gibowicz, 'Stress drop and aftershocks', *Bull. seism. soc. Am.* **63**, 1933–1446 (1973).
79. W. Thatcher, 'Regional variations of seismic source parameters in the Northern Baja California area', *J. geophys. res.* **77**, 1649–1565 (1972).
80. T. C. Hanks and M. Wyss, 'The use of body-wave spectra in the determination of seismic source parameters', *Bull. seism. soc. Am.* **62**, 561–589 (1972).
81. M. Wyss and P. Molnar, 'Efficiency, stress drop, apparent stress, effective stress and frictional stress of Denver, Colorado earthquakes', *J. geophys. res.* **77**, 1433–1438 (1972).
82. J. Fletecher, J. Boatwright, L. Haar, T. Hanks and A. McGarr, 'Source parameters for aftershocks of the Oroville, California, earthquake', *Bull. seism. soc. Am.* **74**, 1101–1123 (1984).
83. J. C. Savage, 'Relation of corner frequency to fault dimensions', *J. geophys. res.* **77**, 3788–3795 (1972).
84. M. Wyss and J. N. Brune, 'Seismic moment, stress and source dimensions for earthquakes in California–Nevada region', *J. geophys. res.* **73**, 4681–4694 (1968).
85. J. G. Anderson, *Strong Motion Seismology*, in Contributions in Seismology, AGU, Washington, DC, 1991.